Pure Rotational Spectroscopy of the CH2CN Radical Extended to the Sub-Millimeter Wave Spectral Region

Olivia Chitarra, Olivier Pirali, Jean-Thibaut Spaniol, Thomas Hearne, Jean-Christophe Loison, John Stanton, Marie-Aline Martin-Drumel

Pure rotational spectroscopy of the CH_2CN radical extended to the sub-millimeter wave spectral region

Olivia Chitarra[a,*], Olivier Pirali[a], Jean-Thibaut Spaniol[a], Thomas Hearne[a], Jean-Christophe Loison[b], John F. Stanton[c], Marie-Aline Martin-Drumel[a,**]

[a] *Université Paris-Saclay, CNRS, Institut des Sciences Moléculaires d'Orsay, 91405 Orsay, France*
[b] *Université Bordeaux, CNRS, Institut des Sciences Moléculaires, 33400 Talence, France*
[c] *Quantum Theory Project, Department of Chemistry, University of Florida, Gainesville, Florida 32611, USA*

Abstract

We present a thorough pure rotational investigation of the CH_2CN radical in its ground vibrational state. Our measurements cover the millimeter and sub-millimeter wave spectral region (79–860 GHz) using a W-band chirped-pulse instrument and a frequency multiplication chain-based spectrometer. The radical was produced in a flow cell at room temperature by H abstraction from acetonitrile using atomic fluorine. The newly recorded transitions of CH_2CN (involving N'' and K_a'' up to 42 and 8, respectively) were combined with the literature data leading to a refinement of the spectroscopic parameters of the species using a Watson S-reduced Hamiltonian. In particular, the A rotational constant and K-dependent parameters are significantly better determined than in previous studies. The present model, which reproduces all experimental transitions to their experimental accuracy, allows for confident searches for the radical in cold to warm environments of the interstellar medium.

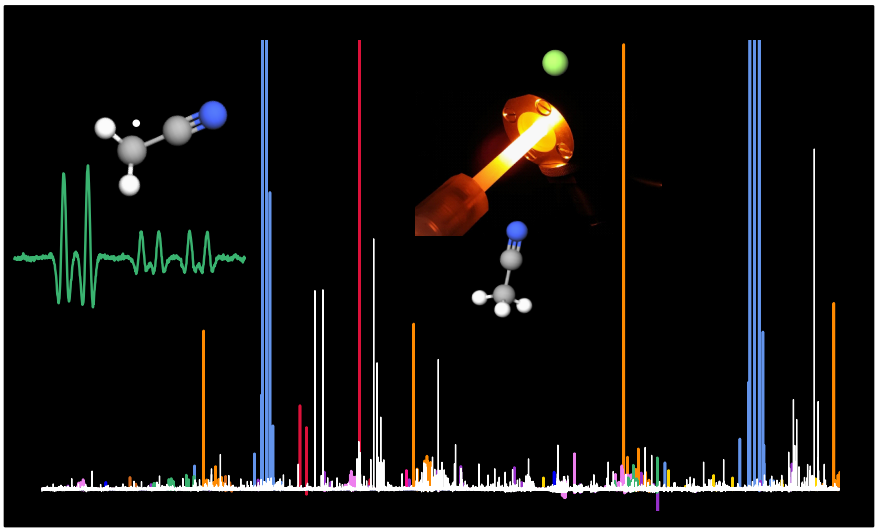

This article has been submitted to *J. Phys. Chem. A* in June, 2022.

*olivia.chitarra@universite-paris-saclay.fr
**marie-aline.martin@universite-paris-saclay.fr

1. Introduction

The cyanomethyl radical, CH_2CN, is a well-studied species because of its importance in many physical and chemical fields. For example, the radical is suspected to be produced by combustion processes in pyrrole [1] and biofuel [2]. Numerous chemical reactions leading to the formation of the CH_2CN radical, mainly from acetonitrile, CH_3CN, have been investigated both experimentally and theoretically. For example, ion-molecule reactions (e.g., $CH_3CN^+ + CH_3CN$ [3]), radical-molecule reactions (e.g., $CH_3CN + OH$ [4]), pyrolysis (e.g., of C_2H_5CN [5]), irradiation (e.g., by γ-rays [6]), and reactions with halogens (e.g., with fluorine atoms [7]) have been documented. From these works, chemical parameters such as the energy barriers, the potential energy surfaces, or the enthalpies of the various reactions studied were derived. CH_2CN reactivity has also attracted significant focus; for instance it has been proposed to react with HCO to form cyanoacetaldehyde in space [8]. Additional investigations have focused on the molecular properties of this carbon-centered radical, such as its geometry [9, 10], electronic structure [11, 12], and stabilization energy [13].

Spectroscopic studies have been carried out on CH_2CN since the 1960's [14]. Early electron paramagnetic resonance investigations in solution have provided isotropic hyperfine coupling constants and g-factor values [15]. Later, gas phase photoelectron spectroscopy has allowed for the determination of the radical electron affinity [16] and its ionization energy [17]. Moran et al. [16] have also established that the radical is planar and belongs to the C_{2v} point group of symmetry; they additionally derived vibrational energies and the first values of the A, B, and C rotational constants of CH_2CN in its vibrational ground state. Experimental vibrational investigations are rather scarce. In matrix, several bands observed in the photolysis of CH_3CN and the reaction of CH_3CN with excited Ar have been tentatively assigned to the CH_2CN radical by Jacox [18]. Quantum chemical calculations enabled definite assignments in the work of Cho and Andrews [19]. A single gas phase investigation of a vibrational band, namely ν_5 (CH_2 wagging), has been reported at high resolution to date [20]. The first pure rotational study in the vibrational ground state was performed in the millimeter-wave region [21] and subsequently extended by Saito and Yamamoto [9]. The authors reported the measurement of transitions from 80 GHz to 280 GHz leading to the determination of rotational, fine, and hyperfine constants. Finally, Ozeki et al. [22] extended the measurement down to the microwave spectral region (20–80 GHz) to refine the hyperfine constants. Since the permanent dipole moment of CH_2CN lies along the a-axis [11], only a-type transitions can be recorded by pure rotation spectroscopy complicating the determination of the A constant and of the Δ_K centrifugal distortion (CD) constant. Consequently, in the fits, A was crudely determined ($A = 284981(115)$ MHz in Saito and Yamamoto [9] and fixed to that value in the following studies) and Δ_K was fixed to a numerical value determined previously for a species similar in size, ketene (H_2CCO [23]).

Using the initial pure rotational investigation [21], CH_2CN was readily detected in the interstellar medium (ISM) by Irvine et al. [24] toward TMC-1 and Sgr B2. Since then, the radical has been detected in another molecular cloud (L483 [25]), a carbon-rich star (IRC +10216 [26]), a prestellar core (L1544 [27]), a protostar (L1527 [28]), and, very recently, in a protoplanetary disk (around the T Tauri star TW Hya [29]. In these sources, CH_2CN exhibits rotational temperatures ranging from 5 to 50 K and transitions as high as 241 GHz have been detected. It is also worth noting that the CHDCN radical has recently been detected toward TMC-1 [30]. The wide distribution of CH_2CN in the ISM has yielded significant focus onto its implication in astrochemical networks. The radical formation (gas phase versus ice grains chemistry [31, 32, 29]) as well as its reactivity, in particular its role in the formation of complex organic molecules [33, 34, 35, 36, 8, 37], have been studied.

Nowadays, radiotelescopes such as ALMA and NOEMA offer a large spectral coverage ($\sim$ 80–950 GHz and $\sim$ 80–360 GHz, respectively). Considering that the pure rotational spectrum of CH_2CN remains intense at frequencies above 300 GHz, even at low temperatures, and that, for species with only a few heavy atoms, the frequency extrapolation toward high frequencies is usually not reliable, new measurements over the sub-millimeter range are warranted [38]. In the laboratory, the relatively high reactivity of radicals hampers their pure rotational spectroscopic studies. In the centimeter-wave spectral region, extremely high sensitivity is achieved by cavity-based Fourier transform microwave (FTMW) spectrometers associated with pulsed-discharge supersonic molecular beams [39,

40]. At higher frequencies, absorption spectrometers based on frequency multiplication chains are widely used in association with various types of radical *in situ* synthesis techniques [41, 42]; although these set-ups do not achieve the sensitivity of FTMW spectroscopy. Recently, chirped-pulse (CP) Fourier transform spectroscopy has revolutionized rotational spectroscopy with its broadband capacities [43]. First and widely used to study molecules with low reactivity [44, 45], it is more and more exploited to investigate reaction dynamics [46] as well as the spectroscopy of reactive species [47, 48]. The joint use of CP and classical narrowband spectrometers has proven particularly efficient in detecting new species [49, 40]. These instrumental developments will undoubtedly prove valuable in enabling new interstellar detections in the millimeter and sub-millimeter [(sub-)millimeter] wave spectral domain [50, 51].

In this work, we have extended the investigation of the room-temperature pure rotational spectrum of the cyanomethyl radical, produced by H-abstraction from CH_3CN using F atoms, in the (sub-)millimeter wave spectral regions (from 75 to almost 900 GHz). 801 lines, including 641 previously unreported (160 are re-measured lines), have been recorded using a broadband CP spectrometer (75–110 GHz) and a widely tunable single-frequency absorption spectrometer exploiting a frequency multiplication chain with a large spectral coverage (140–900 GHz). These transitions have been fitted together with available literature data against a Watson Hamiltonian in the S-reduction allowing for a refinement of the rotational and centrifugal distortion constants of the species. Our data set allows for confident interstellar searches for the radical over the entire (sub-)millimeter region.

2. Laboratory methods

2.1. Synthesis of CH_2CN

The CH_2CN radical was synthesized using a relatively selective production method based on hydrogen abstraction from CH_3CN by fluorine atoms, a method described in Garcia et al. [52]. Fluorine atoms, produced upstream by a 2450 MHz discharge (20–100 W) in a F_2/He mixture at 5% dilution, were injected into the reaction cell where they collided and reacted with CH_3CN to produce the CH_2CN radical. The process is similar to the one employed in our previous work on the CH_2OH radical produced from CH_3OH [38]. In this work, two reaction cells, adapted to either the CP and frequency multiplication chain-based spectrometers, have been used. To limit recombination reactions, both cells were covered with a fluorinated wax (Halocarbon Wax 1500) and were pumped by a roots blower (Edwards, 250 m^3/h) backed by a chemically-graded pump (PFPE-E2M28, Edwards, 30 m^3/h).

By design, the CP spectrometer is optimized for a ∼70 cm-long cell. For the purpose of this study, a reaction cell of suitable length and 5 cm inner diameter has been developed (see Fig. 1). It consists of a central 30 cm long pyrex tube and two T-shaped window holders allowing for precursor injection and pumping. A gas inlet, off-centered by 20 cm toward the injection side, was used to inject fluorine atoms. Partial pressures for the F_2/He mixture and CH_3CN have been optimized to maximize the intensity of a known CH_2CN line at 80480.5 MHz. The F_2/He mixture and the precursor were injected with partial pressures of about 35 µbar and 6 µbar, respectively. The design of the reaction cell associated with the frequency multiplication chain-based spectrometer is similar, although a longer Pyrex tube (145 cm) equipped with three fluorine gas inlets, each separated by 30 cm, was used (see Fig. 2). The partial pressures of the F_2/He mixture and CH_3CN, optimized on CH_2CN lines, were set to about 30 µbar and 2 µbar, respectively. Compared to our previous publication using this set-up [38], the multiplication of fluorine injection sites lead to an increase of the concentration of radicals in the cell while limiting multiple abstraction reactions for a given partial pressure of the F_2/He mixture.

2.2. Chirped-pulse millimeter-wave spectrometer

The broadband CP FT millimeter-wave spectrometer (BrightSpec, Inc) covers the 75–110 GHz spectral region. For all measurements performed in this work, the High Dynamic Range (HDR) mode of the Edgar acquisition software (developed by BrightSpec) was used. It employs a segmented approach in which the entire 35 GHz range is divided into 1165 segments of 30 MHz bandwidth. The excitation pulse was emitted by a horn antenna, collimated by an off-axis parabolic mirror and transmitted into the cell equipped with two high density polyethylene windows (see Fig. 1). Following the excitation pulse, the resulting free induction decay (FID) was collected using an essentially symmetrical system of an off-axis parabolic mirror and a

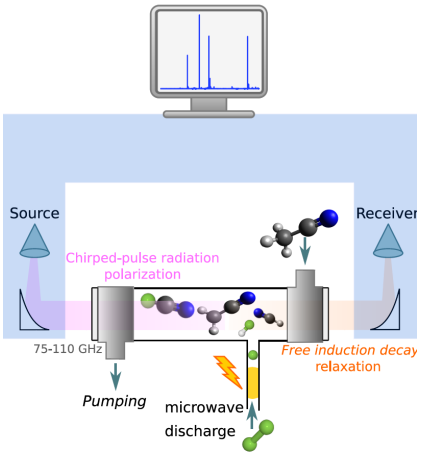

Figure 1: Schematic representation of the experimental set-up using the CP spectrometer (in blue) coupled with the H abstraction method of production. The CH_2CN radical is produced by the reaction between CH_3CN and F atoms produced upstream by a MW discharge. The instrument emits a collimated radiation (in pink) and collects the free induction decay (in orange) by means of two off-axis parabolic mirrors.

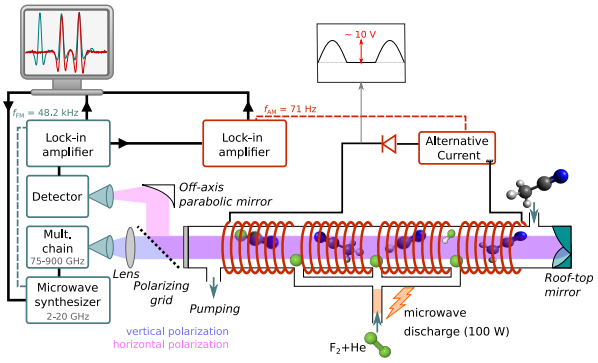

Figure 2: Schematic representation of the upgraded experimental set-up using the frequency multiplication chain-based spectrometer coupled with the H-abstraction method of production. CH_2CN is produced by reaction of CH_3CN with F atoms produced upstream by a MW discharge. The frequency modulated radiation is emitted by a horn antenna and collimated by a 10 cm focal-length Teflon hemispherical lens. Vertical (incident) and horizontal (reflected by the roof-top mirror) polarized radiations are represented in blue and pink, respectively. The roof-top mirror, located at the right-end of the cell, is tilted by 45° from the vertical axis. The off-axis parabolic mirror focuses the radiation onto the detector (Schottky diode or bolometer). An alternating magnetic field (inducing a splitting of the rotational levels of open-shell species by Zeeman effect) is created by an alternating current circulating in a coil (about 800 spirals total) surrounding the cell. The detected signal is demodulated by a first lock-in at the source frequency modulation then demodulated by a second lock-in at the frequency of the modulated magnetic field. Signals are retrieved after each demodulation stage.

horn antenna. By optimizing the intensity of the transition of CH_2CN at 80480.5 MHz, a pulse duration of 250 ns was chosen to polarize the sample. To retrieve the frequency domain spectrum, the FIDs were Fourier transformed over a 4000 ns duration starting 100 ns after the end of the excitation pulse and using a Kaiser-Bessel apodization function. In these conditions, the line profile is dominated by the instrument function resulting in typical full width at half maximum (FWHM) of 600 kHz, larger than the Doppler width of CH_2CN transitions in that range (about 200 kHz at room temperature).

The acquisition procedure consisted of the recording of three distinct spectra. The first spectrum, of 2 millions averaged FIDs (about 4 h of acquisition time), was recorded with the MW discharge switched ON. In these conditions, fluorine atoms are produced and can react with the precursor to produce the radical of interest. To distinguish between transitions arising from open- and closed-shell species, a second spectrum is recorded with the same number of averages with a cylindrical permanent magnet placed underneath the interaction zone where fluorine atoms collide with the precursor. The presence of the permanent magnet, generating a magnetic field of about 140 G, induces a splitting of the energy levels of open-shell species by the Zeeman effect resulting in a significantly modified line profiles (from broader, weaker lines to total visual disappearance of the transitions). Finally, we recorded a reference spectrum of 1 million averages in absence of MW discharge to easily identify the lines of the precursor. Fig. 3 presents the two spectra recorded in presence of fluorine atoms after removal of the contributions of the precursor and possible contaminants lines using the reference spectrum. Therefore, all visible transitions arise from species synthesized by reactions between CH_3CN and fluorine atoms. The red and blue traces correspond to the spectra recorded without and with the permanent magnet, respectively. Lines visible only on the red trace arise from open-shell species. The spectra are quite dense with about 1450 transitions arising from reaction products. In the middle panel of Fig. 3, the same spectra are displayed using a logarithmic scale revealing the high density of lines. Zooms over the two regions where transitions arising from CH_2CN are clearly visible are presented in the lowest panels of Fig. 3. The experimental traces are compared with a simulated stick spectrum of CH_2CN. The experiment is thus able to rapidly (within a few hours) identify open shell

species over a broad spectral range.

2.3. Frequency multiplication chain-based (sub-)millimeter spectrometer

Numerous new pure rotational transitions of the CH_2CN radical were recorded using a (sub-)millimeter-wave spectrometer based on a frequency multiplication chain in the 140–860 GHz spectral region. The experimental set-up has been upgraded compared to our previous publication [38] to allow for a double absorption pathlength, a triple fluorine injection, and a double modulation acquisition procedure (see Fig. 2). The spectrometer combines a radio-frequency synthesizer, locked onto a rubidium atomic clock (Stanford Research Systems), with a solid state frequency multiplication chain (Virginia Diode Inc., VDI) covering the spectral range of interest. The collimated radiation, emitted with a vertical polarization, passed a wire grid polarizer (5 µm diameter and 22 µm spacing wires, PureWavePolarizers Ltd.) before entering the 2 m long Pyrex absorption cell through a Teflon window. On the back port of the cell, a 45° rotated vertical roof-top mirror reflected the radiation back into the cell with horizontal polarization. Once the radiation reached back to the polarizing grid, it was reflected toward an off-axis parabolic mirror which focused the radiation onto a detector. Depending on the spectral range, we used either a Schottky diode detector (140–220 GHz and 220–330 GHz, VDI) or a liquid helium-cooled InSb hot electron bolometer detector (Infrared Labs) operating at 4 K for higher frequencies. A lock-in amplifier (Ametek 7230 DSP) performed signal recovery at the second harmonic. For all measurements, a frequency modulation set to 48.157 kHz was used. To account for Doppler broadening of the lines with increasing frequency while maintaining a relatively constant number of points per line, the frequency steps were set to values ranging from 50 kHz to 200 kHz. The frequency modulation depth was adjusted accordingly from 240 kHz to 1400 kHz. In conventional frequency modulation measurements, the time constant was fixed to 10 ms, and multiple averages, ranging from 10 to 160 averages, were performed in the acquisition software to achieve a total acquisition integration time from 100 ms to 1.6 s for each frequency step.

We made use of the Zeeman modulation to distinguish transitions arising from closed and open-shell species as previously implemented by Amano and Hirota [53]. To generate an amplitude modulated magnetic field, we wrapped a coil of about 800 spirals around the cell (over 1.3 m lengthwise, see Fig. 2). A waveform generator (5 MHz Generator, MLTX 3240, Metrix) generated a 50–100 Hz sinusoidal waveform of 1 V amplitude. The voltage was then amplified by an audio amplifier (X800 MOSFET, Analogue Associates) to reach 10 V (peak to peak) of output voltage. The signal was filtered by a diode that truncated the sinusoidal alternating current so that only positive signal remained and the resulting half-wave rectified current circulated in the coil. A resistor of 1 Ω was added in the circuit in series with the coil yielding a total resistance of 6.5 Ω, resulting in a magnetic field of about 12 Gauss. The FM-demodulated signal output by the first lock-in is sent straight to a second lock-in for the detection of an amplitude modulated signal induced by the alternating magnetic field. In these dual-demodulation experiments, the time constant of the second lock-in was 100 ms. The acquisition program allows for simultaneous signal acquisition at the first (Frequency Modulation, FM) and second (FM + Magnetic Field Modulation, FM+MFM) demodulation stages. On the FM+MFM traces, only transitions arising from open-shell species are visible. An example of the resulting traces recorded around 341915 MHz is presented in Fig 4, where the FM trace is plotted in green (upper panel) and the FM+MFM trace in red (lower panel). On the upper panel, transitions arising from all absorbing species in the range are detected while, on the lower one, all observed transitions are assigned to the ${}^{\Delta K_a}\Delta N_{K_a''}(N'')={}^{Q}R_2(16)$ and ${}^{Q}R_3(16)$ rotational transitions of the CH_2CN radical (pink and blue boxes, respectively). The remaining transitions on the upper panel are unassigned to date (absent the CDMS and the JPL spectral catalogs [54, 55]). The figure hence highlights the straightforward discrimination of open- and closed-shell species.

In total, 756 lines of CH_2CN have been measured and assigned to 5109 rotational transitions (due to unresolved splittings, see spectroscopic section). We estimated the frequency accuracy for each line based on its SNR (ranging from 5 to 130), FWHM, and frequency step [56]; it varies from 50 kHz (intense and isolated lines) to 600 kHz (weak or blended transitions).

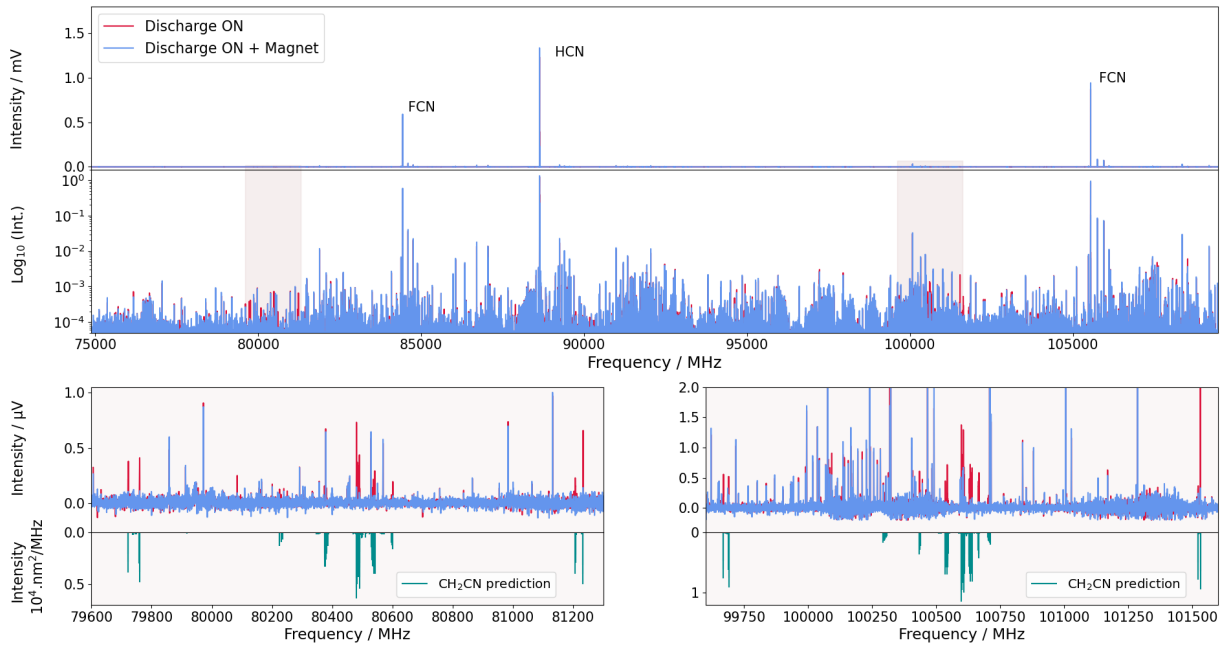

Figure 3: Experimental spectra recorded using the CP spectrometer recorded in presence of fluorine atoms without (red trace) and with (blue trace) the permanent magnet. For the sake of clarity, all transitions arising from the precursor (CH_3CN) have been removed from both spectra. *(Upper panels)* Broadband spectra over the 75–110 GHz spectral region in linear (uppermost) and logarithmic (middle) scales. *(Lower panels)* Two zoomed-in portions of the spectrum around 80 GHz (bottom left) and 100 GHz (bottom right). They both display clusters of transitions of CH_2CN involving $N'' = 3$ (left) and $N'' = 4$ (right). Experimental traces are compared with a simulated stick spectrum of CH_2CN (green trace) performed using the final set of spectroscopic parameters.

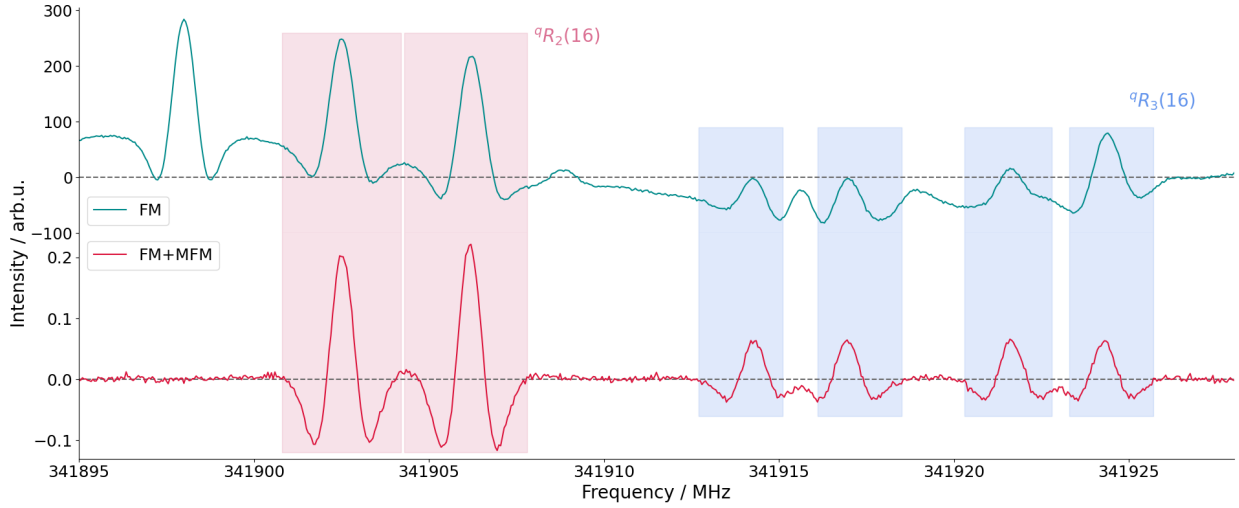

Figure 4: Experimental traces obtained by extracting the signal after each demodulation stage (FM in green, upper panel, and FM+MFM in red, lower panel) around 341915 MHz. The two dashed lines are traced at zero intensity for both signal to allow for the visual inspection of the baseline. The two lines surrounded by pink boxes have been assigned to the $^{Q}R_2(16)$ rotational transitions and the four ones surrounded by blue boxes have been assigned to the $^{Q}R_3(16)$ rotational transitions of the CH_2CN radical. We note that the different intensities for ortho (in pink) and para (in blue) transitions are visible on the figure.

2.4. Spectroscopic description

The cyanomethyl radical, in its $^2B_1$ electronic ground state, is a planar molecule belonging to the C_{2v} point group [16]. The permanent dipole moment lies along the a-axis and takes a value of 3.5 Debye [22]. Consequently, pure rotational transitions are all a-type ($\Delta K_a = K'_a - K''_a = 0$). The radical is an asymmetric top rotor close to the prolate limit with an asymmetry parameter $\kappa = (2B - A - C)/(A - C) = -0.99$ [21].

In the vibronic ground state, the following Hamiltonian can be used to describe the energy levels of the radical:

$$\hat{H} = \hat{H}_{\rm rot} + \hat{H}_{\rm sr} + \hat{H}_{\rm hfs}({\rm N}) + \hat{H}_{\rm hfs}({\rm H}) \qquad (1)$$

where $\hat{H}_{\rm rot}$ is the rotational Hamiltonian (A, B and C rotational constants and centrifugal distortion constants), $\hat{H}_{\rm sr}$ is the spin-rotation (sr) Hamiltonian (one unpaired electron), $\hat{H}_{\rm hfs}$(N) and $\hat{H}_{\rm hfs}$(H) are the hyperfine structure (hfs) Hamiltonians accounting for the non-zero nuclear spin nuclei N ($I_{\rm N} = 1$) and the two equivalent H (H_1 and H_2 with $I_{\rm H_1} = I_{\rm H_2} = 1/2$).

Rotational levels are labeled using the N, K_a and K_c quantum numbers. Each rotational level is split into two sublevels (fine structure), because of the electron spin-rotation coupling, labeled with the J quantum number. Each set of fine structure levels are further split into hyperfine sublevels because of the interaction between nuclear spins. Because $I_{\rm N} = 1$, all levels are split into three sublevels labeled using the F_1 quantum number. The presence of the two equivalent hydrogens leads to values of $I_{\rm H} = I_{\rm H_1} \pm I_{\rm H_2} = 1$ or 0. Rotational levels with even values of K_a (ortho states) are associated with $\mathbf{I}_{\rm H} = 1$ and are split into three sublevels (described with the F quantum number) by hydrogen hyperfine interaction. Rotational levels with odd values of K_a (para states) are associated with $\mathbf{I}_{\rm H} = 0$ and remain unsplit. In consequence, a pattern of nine sublevels is observed for ortho states, described by six quantum numbers: N, K_a, K_c, J, F_1, F while a pattern of three sublevels is observed for para levels described by five quantum numbers: N, K_a, K_c, J, F_1. We note that the splitting due to both hydrogens is larger than the one caused by the nitrogen. However, since we used the CALPGM suite of programs [57] for the analysis and the fit, which requires equivalent nuclei to be coupled last, we used the following coupling scheme:

$$\begin{aligned} \mathbf{N} + \mathbf{S} &= \mathbf{J}, \\ \mathbf{J} + \mathbf{I}_{\rm N} &= \mathbf{F}_1, \\ \mathbf{I}_{\rm H_1} + \mathbf{I}_{\rm H_2} &= \mathbf{I}_{\rm H}, \\ \mathbf{F}_1 + \mathbf{I}_{\rm H} &= \mathbf{F}. \end{aligned} \qquad (2)$$

An example of the hyperfine splittings of an ortho transition is presented in Fig. 5 together with expected line positions when considering successive splittings. Even though the hyperfine components are not fully resolved for this transition under our experimental conditions, the recorded spectrum still nicely reflects the complex structure of the pure rotational spectrum of CH_2CN.

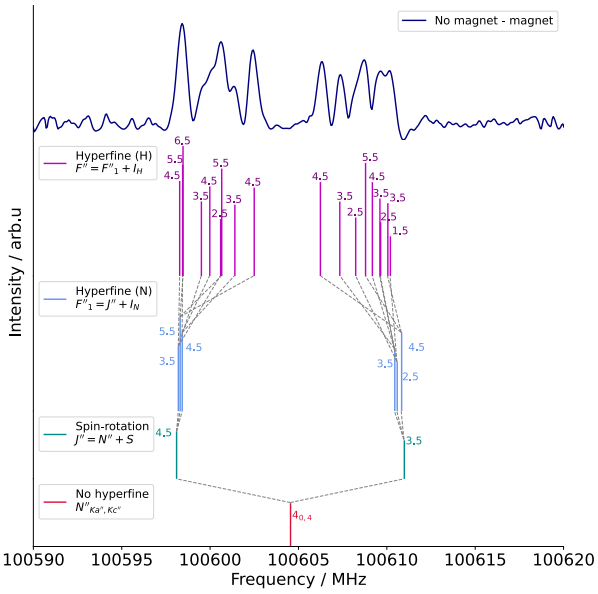

Figure 5: Schematic representation of successive splittings for the $^QR_0(4)$ rotational transition of the CH_2CN radical compared with the experimental trace recorded with the CP spectrometer around 100605 MHz (in dark blue). The experimental trace is a subtraction of the spectrum recorded without the permanent magnet by the one recorded with the magnet. This allows the removal of contributions arising from closed-shell species. Below the experimental trace, predictions of line positions are presented using models including successive couplings.

2.5. Quantum chemical calculations

Quantum-chemical calculations of the molecular parameters relevant to this experiment were done using coupled-cluster theory. Specifically, the all-electron core-correlating cc-pCVTZ and cc-pCVQZ basis sets [58] were used in conjunction with the CCSD(T) treatment of electron correlation [59].

The structure of CH_2CN was optimized with each basis set, and the resulting equilibrium geometries were used in calculations of the molecular properties. The calculated properties comprise the dipole moment, quartic and sextic centrifugal distortion constants, hyperfine constants, electron and nuclear spin-rotation constants [60], and harmonic vibrational frequencies. Using the methods of second-order vibrational perturbation theory (VPT2) [61], the ground state averaged dipole moment was calculated, along with ground state rotational constants. The latter applies vibrational and centrifugal corrections calculated with VPT2 to the equilibrium constants that are directly proportional to the inverse principal moments of inertia. A good summary of the methodology used in this work can be found in Puzzarini et al. [62]. All calculations used the CFOUR program suite [63].

3. Results and discussion

3.1. Chirped-pulse measurements

Despite a rather selective method of production for the CH_2CN radical, many other species were synthesized by the reaction between fluorine atoms and the precursor (CH_3CN) leading to a rich spectrum captured by the broadband CP instrument. The strongest transitions, largely dominating the spectra and clearly visible in the upper panel of Fig. 3, are a triplet lying around 88632 MHz easily assigned to the HCN molecule in its vibrational ground state [64]. Two other strong lines around 84432 and 105539 MHz are assigned to FCN [65]. On In Fig. 6, the experimental trace is the spectrum recorded without the permanent magnet. Similarly to Fig. 3, all contributions from the precursor have been removed using the reference (MW discharge switched off) spectrum. Consequently, all observed transitions arise from species synthesized in the experiment, closed-shell as well as open-shell molecules. The experimental trace is normalized to the most intense transition at 88631.8 MHz (HCN). To assign the spectrum, we first queried the Splatalogue database [66] itself querying JPL and CDMS spectral catalogs [55, 54]. For fluorinated species, we used literature data on species we thought could be present in the set-up. All assigned transitions are plotted in color, the unassigned ones remain in black; for the sake of clarity, the lower panel of Fig. 6 displays these transitions only. The same color is used to plot pure rotational transitions of all variants of a given molecule: within the vibrational ground and excited states as well as isotopologues. A summary of all assignments is provided in Table 1. With the employed method of production, dehydrogenated species from acetonitrile were expected, namely CH_2CN, HCCN and C_2N. Indeed, we observe spectroscopic features unambiguously assigned to CH_2CN (in green on Fig. 6). For HCCN, a single extremely weak, magnet dependent feature is present around 87767.5 MHz which is insufficient for any definite assignment. No C_2N transitions are detected. Besides H-abstraction, the method is also known for F-addition, for instance CH_2FCN transitions are observed on the spectrum. Interestingly, other products are also present with shorter (HCN, FCN) or longer (HC_3N, FC_3N) heavy atom backbones than the precursor. The presence of COF_2 and HFCO is unambiguous and results from oxygen-contamination in our set-up. As highlighted by the lower panel of Fig. 6, many transitions remain unassigned on the spectrum. Some of these transitions probably arise from other fluorinated species. Currently, in terms of number of transitions, a third of the spectrum has been assigned (around 370 transitions over 1050 total). The assignment can also be expressed in terms of percentage of intensity as previously done in McCarthy et al. [40]. The total intensity is defined as the sum of the intensity of all transitions and for each species the sum of individual transitions intensities is determined (see Table 1). The 35% of transitions assigned on the spectrum corresponds to 91% of the total spectral intensity. Consequently, most of the remaining transitions are relatively weak which complicate their assignment. We note that the number of identified peaks depends on the SNR threshold we arbitrary choose. Because the noise level is not constant over the spectral range, some peaks can be missed (because of their low intensity) and, in return, some noisy signal can be misconstrued as peaks, increasing the number of transitions to assign. Finally, it is worth noting that only a few unassigned transitions arise from open-shell species and all exhibit extremely weak SNR. As seen previously by others [67, 40, 68], this example illustrates the ability of CP spectrometers to capture the molecular composition of complex mixtures on broadband spectra.

3.2. (Sub-)millimeter measurements

Using the frequency multiplication chain-based spectrometer, we followed a line-by-line procedure

Table 1: Summary of the assignments of the CP broadband spectrum

	N° lines[a]	% lines[a]	Sum of intensity[b]	% Intensity[b]	Ref.[c]
Total	1032	100	4.44	100	
HCN[d]	11	1.07	2.05	46.14	[1]
FCN[e]	28	2.71	1.75	39.36	[2]
HC_3N[f]	70	6.78	1.48×10^{-1}	3.34	[3]
CH_2CN	85	8.24	2.31×10^{-2}	0.52	[4]
CH_2FCN	13	1.26	7.83×10^{-3}	0.18	[5]
FC_3N[g]	5	0.48	2.73×10^{-3}	0.06	[6]
HNC	1	0.10	1.29×10^{-3}	0.03	[7]
FCCH	2	0.19	1.66×10^{-3}	0.04	[8]
HFCO	35	3.39	1.88×10^{-2}	0.42	[9]
COF_2	116	11.24	6.03×10^{-2}	1.36	[10]
Assigned	366	35.47	4.06	91.46	
Remaining	666	64.53	0.379	8.54	

[a] Number of frequencies (and %) assigned to a given species synthesized by the MW discharge. [b] Sum of the corresponding intensity (and %) for all transitions assigned to a given species. [c] Literature data used for the assignment: [1] DeLucia and Gordy [64], Zelinger et al. [69], Fuchs et al. [70]. [2] Bogey et al. [65], Tyler and Sheridan [71]. [3] de Zafra [72], Mallinson and de Zafra [73], Creswell et al. [74]. [4] Saito and Yamamoto [9] and this work. [5] Guarnieri and Tolkmit [75]. [6] Tanaka et al. [76]. [7] Saykally et al. [77]. [8] derived from Tyler and Sheridan [71]. [9] Jones and Typke [78]. [10] Carpenter [79]. [d] $v_0, v_2 = 2$, $H^{13}CN$ v_0, $HC^{15}N$ v_0. [e] $v_0, v_1 = 1, v_2 = 1, 2, 3$, $FC^{15}N$ v_0, $F^{13}CN$ v_0. [f] $v_0, v_4 = 1, v_5 = 1, v_6 = 1, v_7 = 1, v_5 = 1 + v_7 = 3, v_6 = 1 + v_7 = 1$, $HC^{13}CCN$ v_0, $HCC^{13}CN$ v_0. [g] $v_0, v_7 = 1$.

to measure CH_2CN transitions resulting in few lines arising from other species being detected. The improvements made to the experimental set-up allowed us to perform an efficient re-investigation of the pure rotational spectrum of the CH_2CN radical. Tripling the injection site of fluorine atoms improved production of the radical, while doubling the path length of the cell in combination with the development of the dual demodulation scheme allowed for the detection of weak lines arising from CH_2CN.

Besides the CH_2CN radical, several others species were produced (both open and closed shell). Therefore, the double demodulation detection is extremely efficient in discriminating features arising from open-shell species (as seen on Fig. 4). An additional advantage of this modulation scheme is that transitions arising from open-shell species are detected over a flat baseline (Figs. 4 and 7). Fig. 7 displays several transitions of CH_2CN, following the same selection rule ($^QR_1(N)$), spanning the spectral range covered in this study. Both FM (in green) and FM+MFM (in red) traces are plotted. One can notice that that the SNR is weaker on the FM+MFM trace than on the FM one. This is probably due to the magnet not being strong enough to completely shift the split transitions away from the frequency of the un-split transition, resulting in less than 100% effective AM modulation depth. In other words, the magnetic field modulation is not 100% efficient. This phenomena is emphasized when increasing the frequency (and hence the FWHM). Therefore, in this work, the FM+MFM signal was always used to identify lines of the radical but, depending on the line profile, we used either the FM or FM+MFM signal to retrieve the most accurate line frequency possible. It is worth noting that, for the line lying around 830275 MHz, there is a shift between the FM and the FM+MFM traces. This is probably due to a close shell species possessing a transition at a close frequency from the one of the CH_2CN radical. However, the close shell species is not referenced in the Splatalogue database [66].

3.3. Spectroscopic discussion

In this work, transitions were assigned in a multistep procedure. First, we refit the literature data using a Watson S-reduced Hamiltonian in the I^r representation. The initial dataset contains all pure rotational transitions from Saito et al. [21], Saito and Yamamoto [9], Ozeki et al. [22] at the estimated experimental accuracy of 5 kHz for Ozeki et al. [22]

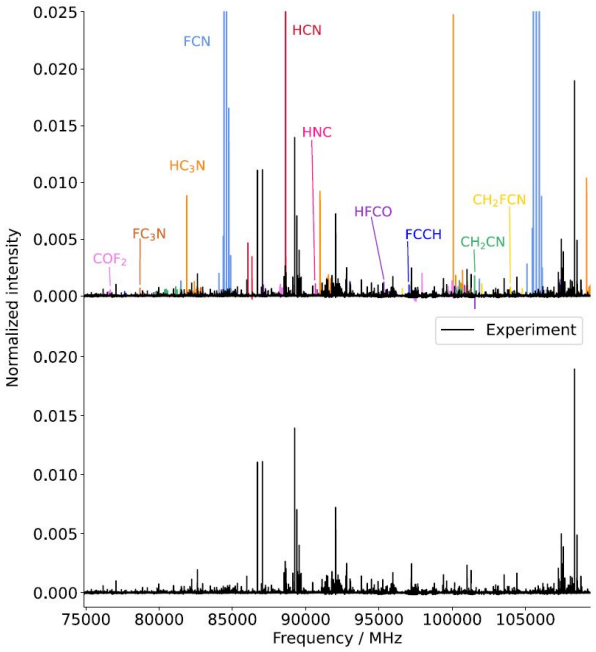

Figure 6: Experimental CP broadband spectrum (black traces) recorded with the MW discharge (without the permanent magnet). For the sake of clarity, all transitions arising from the precursor have been removed. *(Upper panel)* All transitions assigned to various species are plotted in color. *(Lower panel)* Remaining unassigned transitions after the removal of all assigned transitions.

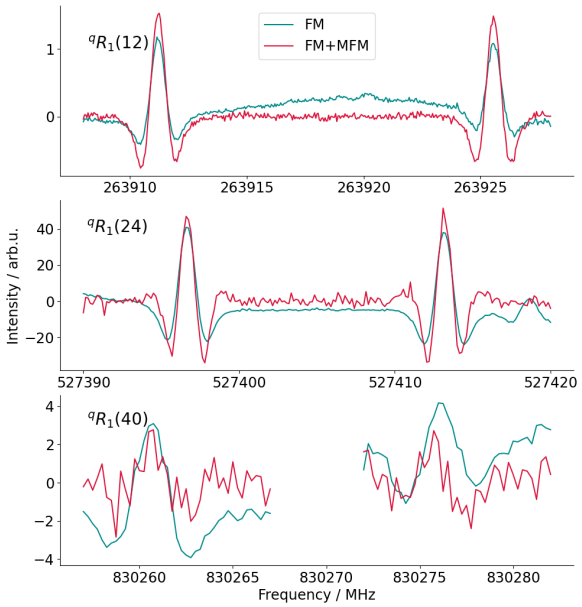

Figure 7: Experimental traces obtained by extracting the signal after the first demodulation stage (FM, in green) and after the second demodulation stage (FM+MFM, in red). *(Upper panel)* Measurement of the $^{Q}R_1(12)$ rotational transition around 263920 MHz, *(middle panel)* $^{Q}R_1(24)$ rotational transition around 527405 MHz and *(lower panel)* $^{Q}R_1(40)$ rotational transition around 830270 MHz.

data and 30 kHz for Saito et al. [21], Saito and Yamamoto [9]. Compared to Ozeki et al. [22] who fit in the A-reduction, we here favored the S-reduction because CH_2CN is close to the prolate limit. We present in table 2 the spectroscopic parameters derived in this work. We refer the reader to the table S1 in the supplementary material for parameters in the A-reduction and a direct comparison with the work of Ozeki et al. [22]. Since the dipole moment lies along the a-axis [11], only a-type pure rotational transitions can be recorded which induces large error bars on the determination of the A rotational constant and for all "K" dependent parameters. In our refit, we fixed A, D_K, and all parameters that could not be properly determined to their calculated value (hence, Δ_K, is no longer fixed to the calculated value of ketene). In addition, we favored a rather constrained fit by keeping all sextic CD constants, but H_{KN}, and the three C_{aa}(N), C_{bb}(N), C_{cc}(N) constants fixed to their calculated values. In addition, while both electron-spin rotation centrifugal distortion constants $D_S(K)$ and $D_S(KN)$ were used in the literature, here $D_S(KN)$ has proven of very little influence in the fit and was thus not included. This model allows the reproduction of literature data relatively well with a root mean square (rms) of 44 kHz and a weighted standard deviation of 2.16, and served as a reliable ground for the new assignments.

In total, we measured 801 frequencies corresponding to 5260 transitions in the linelist. The newly measured transitions, involving N" and K_a'' up to 42 and 8, respectively (compared to 13 and 6 previously), allow for a refinement of the spectroscopic parameters (Table 2). In case of partially resolved structure, the central frequency of the feature is used in the fit and corresponding hyperfine transitions are weighted according to their calculated intensity at 300 K. The A rotational constant is relatively confidently determined accounting for the fact that only a-type transitions are observed. The current value of 284994.2 (39) MHz differs by 13 MHz (0.005%) from the literature data, well within the error bar given by Saito and Yamamoto [9], and is 30 times better determined. There is also a significant improvement of the CD

Table 2: Spectroscopic parameters (in MHz, unless otherwise noted) of CH_2CN in the Watson S-reduction calculated in this work and determined in the refit of the literature (Refit) and after including the present measurements (Final). Numbers in parentheses are one standard deviation in units of the least significant figure.

Parameters [a]		Calc.[b]	Refit[c]	Final
Rotational parameters				
A		285022	285022	284994.4 (39)
B		10248	10246.22630 (42)	10246.23330 (38)
C		9877	9876.56830 (42)	9876.56149 (36)
Rotational centrifugal distortion constants				
D_N	$\times 10^3$	3.79	3.95221 (90)	3.95500 (15)
D_{NK}		0.429	0.416451 (97)	0.415810 (53)
D_K		20.7	20.7	20.7
d_1	$\times 10^3$	−0.140	−0.140	−0.16338 (16)
d_2	$\times 10^3$	−0.0374	−0.0374	−0.04670 (15)
H_N	$\times 10^9$	−1.08	−1.08	−1.08
H_{NK}	$\times 10^6$	3.19	3.19	3.480 (38)
H_{KN}	$\times 10^3$	−1.05	−0.7075 (78)	−0.8449 (45)
H_K	$\times 10^3$	5.86	5.86	5.86
h_1	$\times 10^{11}$	1.70	1.70	1.70
h_2	$\times 10^{10}$	3.93	3.93	3.93
h_3	$\times 10^{11}$	6.32	6.32	6.32
L_{NK}	$\times 10^6$			−0.0278 (18)
L_{KKN}	$\times 10^6$		−8.54 (16)	−0.84 (12)
P_{KKNN}	$\times 10^9$			0.946 (21)
P_{KKKN}	$\times 10^6$			−0.1244 (11)
Electron spin-rotation and higher order terms				
ϵ_{aa}		−697	−661.5169 (93)	−661.5305 (84)
ϵ_{bb}		−23.7	−24.1133 (47)	−24.1120 (46)
ϵ_{cc}		1.43	−2.0412 (47)	−2.0388 (46)
$D_S(K)$			0.0886 (39)	0.0998 (14)
Isotropic and anisotropic hyperfine interaction constants				
a_F(N)		7.19	9.4902 (17)	9.4905 (17)
T_{aa}(N)		−14.8	−15.6448 (33)	−15.6451 (32)
T_{bb}(N)		−13.5	−12.4720 (42)	−12.4734 (42)
χ_{aa}(N)		−4.26	−4.1964 (40)	−4.1959 (40)
χ_{bb}(N)		1.89	1.8199 (60)	1.8168 (60)
C_{aa}(N)		−0.0275	−0.0275	−0.0275
C_{bb}(N)		−0.0021	−0.0021	−0.0021
C_{cc}(N)		−0.0023	−0.0023	−0.0023
a_F(H)[d]		−56.9	−59.640 (13)	−59.644 (13)
T_{aa}(H)[d]		−17.1	−15.8966 (28)	−15.8965 (28)
T_{bb}(H)[d]		16.0	16.0	16.0
T_{bc}(H)[d]		1.15	1.15	1.15
Relevant fit parameters				
n [e]			545(207)	545(207)+5260(801)
$N''_{\max}$, $K''_{a\,\max}$ [f]			13,6	42,8
rms			0.044	0.147
σ [g]			2.16	1.18

[a] Parameters with no numerical values have not been used in the fit (i.e., fixed to 0); all values without error have been kept fixed to the calculated value, this work. [b] see text. [c] Refit from the data from Saito et al. [21], Saito and Yamamoto [9] and Ozeki et al. [22]. [d] $X(\mathrm{H}) = X(\mathrm{H1}) = X(\mathrm{H2})$ for a given parameter X . [e] Number of fitted transitions (different frequencies). In the final fit, the number of lines from the literature and of newly measured lines are reported, respectively. [f] unitless [g] Weighted standard deviation, unitless

parameters. While it was possible to determine almost all quartic CD terms (D_K remains fixed to the calculated value), only sextic terms (and higher order of magnitude terms) involving both N and K were determined. More specifically, terms involving higher order in K than N (such as H_{KN}, L_{KKN} and P_{KKKN}) have proven of greater importance for the reproduction of transitions involving high values of N and K_a. We note that the L_{KKN} parameter is ten times smaller in the final fit than in the refit, we attribute this difference to the addition of more higher order terms in the final fit. The P_{KKKN} parameter is only almost 10 times smaller than the L_{KKN} parameter probably reflecting anomalous centrifugal distortion. Electron-spin rotation and hyperfine constants are very similar in the refit and final fit, and in excellent agreement with the calculated values. We note that for the electron spin-rotation ϵ_{cc} parameter, the fitted value is of opposite sign compared to the calculated one. Concerning the hyperfine structure, even though it is partly resolved for several transitions (for example see Fig. 5), the error on the corresponding parameters is set by the highly accurate centimeter-wave data. One significant difference with the literature data however is the sign of the $C_{aa}(N)$ parameter (0.0273 MHz in Ozeki et al. [22]). We found that this sign is set positive by four transitions from Ozeki et al. [22] only. All the other data are reproduced within their experimental accuracy using the negative calculated value (−0.0275 MHz). We favored a constrained fit with $C_{aa}(N)$ fixed to its calculated value. In the final fit, the aforementioned four transitions are poorly reproduced (10 σ). Finally, it is worth noting that the CDMS [54] prediction (based on the literature pure rotational data) is quite reliable when extrapolating in N for K_a values previously observed (with experimental frequencies located at 800 GHz lying less than 2 MHz away from the catalog). However, for such a light molecule treated using a semi-rigid rotor model, the extrapolation in K_a is far less reliable. For example, the $^{Q}R_8(14)$ transition (lying around 300905 MHz) is predicted more than 10 MHz away from the experimental measurement.

Overall, the final fit allows the reproduction of the 5805 rotational transitions (1008 different frequencies) at their experimental accuracy with a weighted standard deviation of 1.18 and a rms of 147 kHz. It is worth noting that the weighted standard deviation obtained at the refit stage came from the rather constrained model. A fit of all the available pure rotation data (literature and this work) in the Watson A-reduction is also provided in the supplementary material (Table S1 and ASCII files). This fit is of similar quality to the one in the S-reduction.

4. Conclusion and prospects

In this work, we re-investigated the pure rotational spectrum of the cyanomethyl radical, CH_2CN, from 75 GHz to almost 900 GHz. The radical was produced by hydrogen abstraction from acetonitrile with fluorine atoms. To record its rotational transitions, we used two spectrometers: a newly available CP instrument and a frequency multiplication chain-based spectrometer that has been upgraded (double pass, triple F injection and double modulation) to improve its sensitivity compared to a similar instrument used in a previous study. Our set-ups appear complementary: the CP offers a broadband view in the 75–110 GHz range while the frequency multiplication chain is highly tunable up to 900 GHz. In addition to CH_2CN lines, many transitions arising from other species have been observed, several of them remaining unassigned to date. The CP set-up is promising for future studies of reactive species. Concerning the second spectrometer, the double modulation procedure has proven extremely efficient in quickly identifying transitions arising from the CH_2CN radical.

With these set-ups, transitions of CH_2CN, involving N'' up to 42 and K_a'' up to 8, have been measured and added to the literature data leading to a refinement of the spectroscopic parameters describing the species. Currently, the most recent detection of the radical in the ISM [29] was performed using transitions lying around 240 GHz. Since the rotational spectrum of CH_2CN extends well above this frequency even at mild rotational temperature (see Fig. S1 in the supplementary material), the present work may help future detection using current astronomical observatories from cold to warm environments of the ISM and up to the terahertz range.

Supporting Information

- fit files in ascii format (both *A*- and *S*-reduction)
- Simulation of the pure rotational spectrum of the radical calculated at different temperatures.
- Table of the spectroscopic parameters in the Watson *A*-reduction.

Acknowledgments

This project received funding from the *Région Ile-de-France*, through DIM-ACAV$^+$, from the *Agence Nationale de la Recherche* (ANR-19-CE30-0017-01), from the "*Investissements d'Avenir*" LabEx PALM (ANR-10-LABX-0039-PALM), and from the *Programme National* "*Physique et Chimie du Milieu Interstellaire*" (PCMI) of CNRS/INSU with INC/INP co-funded by CEA and CNES.

References

[1] X. Hong, L. Zhang, T. Zhang, F. Qi, An experimental and theoretical study of pyrrole pyrolysis with tunable synchrotron vuv photoionization and molecular-beam mass spectrometry, The Journal of Physical Chemistry A 113 (2009) 5397–5405. doi:10.1021/jp9002966.

[2] K. Kohse-Höinghaus, P. Oßwald, T. Cool, T. Kasper, N. Hansen, F. Qi, C. Westbrook, P. Westmoreland, Biofuel combustion chemistry: From ethanol to biodiesel, Angewandte Chemie International Edition 49 (2010) 3572–3597. doi:https://doi.org/10.1002/anie.200905335.

[3] H. Tachikawa, T. Fukuzumi, K. Inaoka, I. Koyano, Electronic state dependence of the ion–molecule reaction $CH_3CN^+ + CH_3CN \rightarrow CH_4CN^+ + CH_2CN$: threshold electron–secondary ion coincidence (tesico) and direct ab initio molecular dynamics study, Phys. Chem. Chem. Phys. 12 (2010) 15399–15405. doi:10.1039/C004202A.

[4] Q.-S. Li, C. Y. Wang, Direct dynamic study on the hydrogen abstraction reaction CH_3CN + oh $\rightarrow$ CH_2CN + H_2O, Journal of Computational Chemistry 25 (2004) 251–257. doi:10.1002/jcc.10194.

[5] A. B. Trenwith, Pyrolysis of propionitrile and the resonance stabilisation energy of the cyanomethyl radical, J. Chem. Soc., Faraday Trans. 1 79 (1983) 2755–2764. doi:10.1039/F19837902755.

[6] P. B. Ayscough, R. G. Collins, T. J. Kemp, Electron spin resonance studies of fundamental processes in radiation and photochemistry. ii. photochemical reactions in γ-irradiated nitriles at 77 k, The Journal of Physical Chemistry 70 (1966) 2220–2223. doi:10.1021/j100879a023.

[7] S. Pratihar, X. Ma, J. Xie, R. Scott, E. Gao, B. Ruscic, A. J. A. Aquino, D. W. Setser, W. L. Hase, Post-transition state dynamics and product energy partitioning following thermal excitation of the f...HCH_2CN transition state: Disagreement with experiment, The Journal of Chemical Physics 147 (2017) 144301. doi:10.1063/1.4985894.

[8] B. Ballotta, S. Nandi, V. Barone, S. Rampino, Gas-phase formation and isomerization reactions of cyanoacetaldehyde, a prebiotic molecule of astrochemical interest, ACS Earth and Space Chemistry 5 (2021) 1071–1082. doi:10.1021/acsearthspacechem.1c00013.

[9] S. Saito, S. Yamamoto, The microwave spectrum of the cyanomethyl radical $CH_2CN(^2b_1)$, The Journal of Chemical Physics 107 (1997) 1732–1739. doi:10.1063/1.475154.

[10] D. E. Woon, E. Herbst, Quantum chemical predictions of the properties of known and postulated neutral interstellar molecules, The Astrophysical Journal Supplement Series 185 (2009) 273–288. doi:10.1088/0067-0049/185/2/273.

[11] A. Hinchliffe, Electronic structure and properties of CH_2CN and CH_2NC, Journal of Molecular Structure 53 (1979) 147–149. doi:https://doi.org/10.1016/0022-2860(79)80335-X.

[12] F. Delbecq, Structure and reactivity of the CH_2CN radical, Chemical Physics Letters 99 (1983) 21–26. doi:https://doi.org/10.1016/0009-2614(83)80262-0.

[13] D. J. Henry, C. J. Parkinson, L. Radom, An assessment of the performance of high-level theoretical procedures in the computation of the heats of formation of small open-shell molecules, The Journal of Physical Chemistry A 106 (2002) 7927–7936. doi:10.1021/jp0260752.

[14] J. T. Pearson, P. Smith, T. C. Smith, The electron paramagnetic resonance spectra of the 2-cyano-2-propyl radical and related species, Canadian Journal of Chemistry 42 (1964) 2022–2025. doi:10.1139/v64-296.

[15] P. Smith, R. Kaba, T. Smith, J. Pearson, P. Wood, Epr study of radicals formed from aliphatic nitriles, Journal of Magnetic Resonance (1969) 18 (1975) 254–264. doi:https://doi.org/10.1016/0022-2364(75)90124-9.

[16] S. Moran, H. B. Ellis, D. J. DeFrees, A. D. McLean, G. B. Ellison, Carbanion spectroscopy: cyanomethide anion (CH_2CN^-), Journal of the American Chemical Society 109 (1987) 5996–6003. doi:10.1021/ja00254a018.

[17] G. Garcia, J. Krüger, B. Gans, C. Falvo, L. Coudert, J. Loison, Valence shell threshold photoelectron spectroscopy of the ch_xcn (x = 0-2) and cnc radicals., The Journal of chemical physics 147 1 (2017) 013908.

[18] M. E. Jacox, Matrix isolation study of the interaction of excited argon atoms with methyl cyanide, vibrational and electronic spectra of ketenimine, Chemical Physics 43 (1979) 157–172. doi:10.1016/0301-0104(79)85184-8.

[19] H.-G. Cho, L. Andrews, Matrix infrared spectra and density functional calculations of the H_2CCN and H_2CNC radicals produced from CH_3CN, The Journal of Physical Chemistry A 115 (2011) 8638–8642. doi:10.1021/jp204887y.

[20] Y. Sumiyoshi, K. Tanaka, T. Tanaka, Time-resolved infrared diode laser spectroscopy of the ν_5 band of the cyanomethyl radical (H_2CCN), The Journal of

Chemical Physics 104 (1996) 1839–1845. doi:10.1063/1.471709.

[21] S. Saito, S. Yamamoto, W. Irvine, L. Ziurys, H. Suzuki, M. Ohishi, N. Kaifu, Laboratory detection of a new interstellar free radical $CH_2CN(^2b_1)$, The Astrophysical journal 334 (1988) L113–6. doi:10.1086/185324.

[22] H. Ozeki, T. Hirao, S. Saito, S. Yamamoto, Laboratory microwave spectroscopy of the cyanomethyl radical, CH_2CN, The Astrophysical Journal 617 (2004) 680–684. doi:10.1086/425229.

[23] J. Johns, J. Stone, G. Winnewisser, The ground state of ketene, Journal of Molecular Spectroscopy 42 (1972) 523–535. doi:https://doi.org/10.1016/0022-2852(72)90227-5.

[24] W. M. Irvine, P. Friberg, A. Hjalmarson, S. Ishikawa, N. Kaifu, K. Kawaguchi, S. C. Madden, H. E. Matthews, M. Ohishi, S. Saito, H. Suzuki, P. Thaddeus, B. E. Turner, S. Yamamoto, L. M. Ziurys, Identification of the interstellar cyanomethyl radical (ch2cn) in themolecular clouds tmc-1 and sagittarius b2., The Astrophysical Journal Letters 334 (1988) L107–L111. doi:10.1086/185323.

[25] M. Agúndez, N. Marcelino, J. Cernicharo, E. Roueff, M. Tafalla, A sensitive λ 3 mm line survey of l483 - a broad view of the chemical composition of a core around a class 0 object, Astronomy & Astrophysics 625 (2019) A147. doi:10.1051/0004-6361/201935164.

[26] M. Agúndez, J. P. Fonfría, J. Cernicharo, J. R. Pardo, M. Guélin, Detection of circumstellar CH_2CHCN, CH_2CN, CH_3CCH, and $H_2CS\cdot$, Astronomy & Astrophysics 479 (2008) 493–501. doi:10.1051/0004-6361:20078956.

[27] C. Vastel, S. Yamamoto, B. Lefloch, R. Bachiller, Hyperfine structure of the cyanomethyl radical (ch2cn) in the l1544 prestellar core, Astronomy & Astrophysics 582 (2015) L3. doi:10.1051/0004-6361/201527153.

[28] K. Yoshida, N. Sakai, Y. Nishimura, T. Tokudome, Y. Watanabe, T. Sakai, S. Takano, S. Yamamoto, An unbiased spectral line survey observation toward the low-mass star-forming region L1527, Publications of the Astronomical Society of Japan 71 (2019). doi:10.1093/pasj/psy136, s18.

[29] A. Canta, R. Teague, R. L. Gal, K. I. Öberg, The first detection of CH_2CN in a protoplanetary disk, 2021. arXiv:2109.09564.

[30] C. Cabezas, Y. Endo, E. Roueff, N. Marcelino, M. Agúndez, B. Tercero, J. Cernicharo, Space and laboratory observation of the deuterated cyanomethyl radical hdccn, Astron. Astrophys. 646 (2021) L1. doi:10.1051/0004-6361/202040210.

[31] E. Herbst, C. M. Leung, The gas phase production of CH_2CN and other organo-nitrogen species in dense interstellar clouds., Astronomy & Astrophysics 233 (1990) 177–180.

[32] B. E. Turner, P. Friberg, W. M. Irvine, S. Saito, S. Yamamoto, Interstellar cyanomethane, The Astrophysical Journal 335 (1990) 546–561. doi:10.1086/168787.

[33] M. F. Hayley J. Andreazza, J. H. Bowie, The formation of the stable radicals CH_2CN, CH_3CHCN and CH_2CH_2CN from the anions $^-CH_2CN$, $^-CH_3CHCN$ and $^-CH_2CH_2CNn$ in the gas phase. a joint experimental and theoretical study, Organic & Biomolecular Chemistry, 4 (2006) 2466–2472. doi:10.1039/b602621d.

[34] D. J. Knowles, T. Wang, J. H. Bowie, Radical formation of amino acid precursors in interstellar regions? ser, cys and asp, Org. Biomol. Chem. 8 (2010) 4934–4939. doi:10.1039/C0OB00232A.

[35] J. Loison, E. Hébrard, M. Dobrijevic, K. Hickson, F. Caralp, V. Hue, G. Gronoff, O. Venot, Y. Bénilan, The neutral photochemistry of nitriles, amines and imines in the atmosphere of titan, Icarus 247 (2015) 218–247. doi:10.1016/j.icarus.2014.09.039.

[36] C. Cabezas, C. Bermúdez, J. D. Gallego, B. Tercero, J. M. Hernández, I. Tanarro, V. J. Herrero, J. L. Doménech, J. Cernicharo, The millimeter-wave spectrum and astronomical search of succinonitrile and its vibrational excited states, Astronomy & Astrophysics 629 (2019) A35. doi:10.1051/0004-6361/201935899.

[37] J. Cernicharo, C. Cabezas, Y. Endo, M. Agúndez, B. Tercero, J. R. Pardo, N. Marcelino, P. de Vicente, The sulphur saga in tmc-1: Discovery of hcscn and hcscch, Astron. Astrophys. 650 (2021) L14. doi:10.1051/0004-6361/202141297.

[38] O. Chitarra, M.-A. Martin-Drumel, B. Gans, J.-C. Loison, S. Spezzano, V. Lattanzi, H. S. P. Müller, O. Pirali, Reinvestigation of the rotation-tunneling spectrum of the CH_2OH radical - accurate frequency determination of transitions of astrophysical interest up to 330 ghz, Astronomy & Astrophysics 644 (2020) A123. doi:10.1051/0004-6361/202039071.

[39] Y. Endo, H. Kohguchi, Y. Ohshima, Pdn–ftmw spectroscopy of open-shell complexes, Faraday Discuss. 97 (1994) 341–350. doi:10.1039/FD9949700341.

[40] M. C. McCarthy, K. L. K. Lee, P. B. Carroll, J. P. Porterfield, P. B. Changala, J. H. Thorpe, J. F. Stanton, Exhaustive product analysis of three benzene discharges by microwave spectroscopy, The Journal of Physical Chemistry A 124 (2020) 5170–5181. doi:10.1021/acs.jpca.0c02919.

[41] S. Yamamoto, S. Saito, The microwave spectra of co in the electronically excited states (a 3π r and a' $3\sigma^+$), The Journal of Chemical Physics 89 (1988) 1936–1944. doi:10.1063/1.455091.

[42] C. Bermudez, S. Bailleux, J. Cernicharo, Laboratory detection of the rotational-tunnelling spectrum of the hydroxymethyl radical, ch2oh, Astron. Astrophys. 598 (2017) A9. doi:10.1051/0004-6361/201629508.

[43] G. G. Brown, B. C. Dian, K. O. Douglass, S. M. Geyer, S. T. Shipman, B. H. Pate, A broadband fourier transform microwave spectrometer based on chirped pulse excitation, Review of Scientific Instruments 79 (2008) 053103. doi:10.1063/1.2919120.

[44] S. A. Peebles, M. M. Serafin, R. A. Peebles, G. A. Guirgis, H. D. Stidham, Rotational spectra and conformational analysis of diethylsilane and diethyldifluorosilane, The Journal of Physical Chemistry A 113 (2009) 3137–3142. doi:10.1021/jp811049n.

[45] M. Fatima, C. Pérez, B. E. Arenas, M. Schnell, A. L. Steber, Benchmarking a new segmented k-band chirped-pulse microwave spectrometer and its application to the conformationally rich amino alcohol isoleucinol, Phys. Chem. Chem. Phys. 22 (2020) 17042–17051. doi:10.1039/D0CP01141J.

[46] K. Prozument, G. Barratt Park, R. G. Shaver, A. K. Vasiliou, J. M. Oldham, D. E. David, J. S. Muenter, J. F. Stanton, A. G. Suits, G. Barney Ellison, R. W. Field, Chirped-pulse millimeter-wave spectroscopy for dynamics and kinetics studies of pyrolysis reactions, Phys. Chem. Chem. Phys. 16 (2014) 15739–15751. doi:10.1039/C3CP55352C.

[47] J. P. Porterfield, K. L. K. Lee, V. Dell'Isola, P. B. Carroll, M. C. McCarthy, Characterization of the simplest hydroperoxide ester, hydroperoxymethyl formate, a precursor of atmospheric aerosols, Phys. Chem. Chem. Phys. 21 (2019) 18065–18070. doi:10.1039/C9CP03466H.

[48] L. Kolesniková, I. León, E. R. Alonso, S. Mata, J. L. Alonso, An innovative approach for the generation of species of the interstellar medium, Angewandte Chemie International Edition 60 (2021) 24461–24466. doi:https://doi.org/10.1002/anie.202110325.

[49] K. N. Crabtree, M.-A. Martin-Drumel, G. G. Brown, S. A. Gaster, T. M. Hall, M. C. McCarthy, Microwave spectral taxonomy: A semi-automated combination of chirped-pulse and cavity fourier-transform microwave spectroscopy, The Journal of Chemical Physics 144 (2016) 124201. doi:10.1063/1.4944072.

[50] C. N. Shingledecker, K. L. K. Lee, J. T. Wandishin, N. Balucani, A. M. Burkhardt, S. B. Charnley, R. Loomis, M. Schreffler, M. Siebert, M. C. McCarthy, B. A. McGuire, Detection of interstellar H_2CCCHC_3N. A possible link between chains and rings in cold cores, Astronomy & Astrophysics 652 (2021) L12. doi:10.1051/0004-6361/202140698.

[51] M. C. McCarthy, K. L. K. Lee, R. A. Loomis, A. M. Burkhardt, C. N. Shingledecker, S. B. Charnley, M. A. Cordiner, E. Herbst, S. Kalenskii, E. R. Willis, C. Xue, A. J. Remijan, B. A. McGuire, Interstellar detection of the highly polar five-membered ring cyanocyclopentadiene, Nature Astronomy 5 (2021) 176–180. doi:10.1038/s41550-020-01213-y. arXiv:2009.13546.

[52] G. A. Garcia, X. Tang, J.-F. Gil, L. Nahon, M. Ward, S. Batut, C. Fittschen, C. A. Taatjes, D. L. Osborn, J.-C. Loison, Synchrotron-based double imaging photoelectron/photoion coincidence spectroscopy of radicals produced in a flow tube: Oh and od, The Journal of Chemical Physics 142 (2015) 164201. doi:10.1063/1.4918634.

[53] T. Amano, E. Hirota, Microwave spectrum of the molecular oxygen in the excited vibrational state, Journal of Molecular Spectroscopy 53 (1974) 346–363. doi:https://doi.org/10.1016/0022-2852(74)90071-X.

[54] C. P. Endres, S. Schlemmer, P. Schilke, J. Stutzki, H. S. Müller, The cologne database for molecular spectroscopy, cdms, in the virtual atomic and molecular data centre, vamdc, Journal of Molecular Spectroscopy 327 (2016) 95–104. doi:https://doi.org/10.1016/j.jms.2016.03.005, new Visions of Spectroscopic Databases, Volume II.

[55] H. M. Pickett, R. L. Poynter, E. A. Cohen, M. L. Delitsky, J. C. Pearson, H. S. P. Müller, Submillimeter, millimeter and microwave spectral line catalog, Journal of Quantitative Spectroscopy and Radiative Transfer 60 (1998) 883–890. doi:10.1016/S0022-4073(98)00091-0.

[56] D. A. Landman, R. Roussel-Dupre, G. Tanigawa, On the statistical uncertainties associated with line profile fitting, The Astrophyscal Journal 261 (1982) 732–735. doi:10.1086/160383.

[57] H. M. Pickett, The fitting and prediction of vibration-rotation spectra with spin interactions, Journal of Molecular Spectroscopy 148 (1991) 371 – 377. doi:https://doi.org/10.1016/0022-2852(91)90393-0.

[58] D. E. Woon, T. H. Dunning, Gaussian basis sets for use in correlated molecular calculations. v. core-valence basis sets for boron through neon, The Journal of Chemical Physics 103 (1995) 4572–4585. doi:10.1063/1.470645.

[59] K. Raghavachari, G. W. Trucks, J. A. Pople, M. Head-Gordon, A fifth-order perturbation comparison of electron correlation theories, Chemical Physics Letters 157 (1989) 479–483. doi:https://doi.org/10.1016/S0009-2614(89)87395-6.

[60] J. GAUSS, D. SUNDHOLM, Coupled-cluster calculations of spin-rotation constants, Molecular Physics 91 (1997) 449–458. doi:10.1080/002689797171346.

[61] I. M. Mills, Vibration-Rotation Structure in Asymmetric- and Symmetric-Top Molecules, in: K. N. Rao, C. W. Mathews (Eds.), Molecular Spectroscopy: Modern Research, Volume 1, 1972, p. 115.

[62] C. Puzzarini, J. F. Stanton, J. Gauss, Quantum-chemical calculation of spectroscopic parameters for rotational spectroscopy, International Reviews in Physical Chemistry 29 (2010) 273–367. doi:10.1080/01442351003643401.

[63] D. A. Matthews, L. Cheng, M. E. Harding, F. Lipparini, S. Stopkowicz, T.-C. Jagau, P. G. Szalay, J. Gauss, J. F. Stanton, Coupled-cluster techniques for computational chemistry: The cfour program package, The Journal of Chemical Physics 152 (2020) 214108. doi:10.1063/5.0004837.

[64] F. DeLucia, W. Gordy, Molecular-beam maser for the shorter-millimeter-wave region: Spectral constants of hcn and dcn, Phys. Rev. 187 (1969) 58–65. doi:10.1103/PhysRev.187.58.

[65] M. Bogey, A. Farkhsi, F. Remy, I. Dubois, H. Bredohl, A. Fayt, Millimeter and submillimeter spectra of cyanogen fluoride, fcn, Journal of Molecular Spectroscopy 170 (1995) 417–423.

[66] NRAO, https://www.cv.nrao.edu/php/splat/advanced.php, 2019.

[67] N. Dias, B. Joalland, N. M. Ariyasingha, A. G. Suits, B. M. Broderick, Direct versus indirect photodissociation of isoxazole from product branching: A chirped-pulse fourier transform mm-wave spectroscopy/pulsed uniform flow investigation, The Journal of Physical Chemistry A 122 (2018) 7523–7531. doi:10.1021/acs.jpca.8b04713.

[68] L. Kolesniková, I. León, E. R. Alonso, S. Mata, J. L. Alonso, An innovative approach for the generation of species of the interstellar medium, Angewandte Chemie International Edition 60 (2021) 24461–24466. doi:https://doi.org/10.1002/anie.202110325.

[69] Z. Zelinger, T. Amano, V. Ahrens, S. Brünken, F. Lewen, H. S. P. Müller, G. Winnewisser, Submillimeter-wave spectroscopy of HCN in excited vibrational states, Journal of Molecular Spectroscopy 220 (2003) 223–233. doi:10.1016/S0022-2852(03)00129-2.

[70] U. Fuchs, S. Bruenken, G. W. Fuchs, S. Thorwirth, V. Ahrens, F. Lewen, S. Urban, T. Giesen, G. Winnewisser, High Resolution Spectroscopy of HCN Isotopomers: $H^{13}CN$, $HC^{15}N$, and $H^{13}C^{15}N$ in the Ground and First Excited Bending Vibrational State, Zeitschrift Naturforschung Teil A 59 (2004) 861–872. doi:10.1515/zna-2004-1123.

[71] J. K. Tyler, J. Sheridan, Structural studies of linear molecules by microwave spectroscopy, Trans. Faraday Soc. 59 (1963) 2661–2670. doi:10.1039/TF9635902661.

[72] R. L. de Zafra, Precise Laboratory Determination of Rotational Transition Frequencies in Cyanoacetylene,

The Astrophysical Journal 170 (1971) 165. doi:10.1086/151198.

[73] P. Mallinson, R. L. de Zafra, The microwave spectrum of cyanoacetylene in ground and excited vibrational states, Molecular Physics 36 (1978) 827–843. doi:10.1080/00268977800101971.

[74] R. A. Creswell, G. Winnewisser, M. C. L. Gerry, Rotational spectra of the ^{13}C and ^{15}N isotopic species of cyanoacetylene., Journal of Molecular Spectroscopy 65 (1977) 420–429. doi:10.1016/0022-2852(77)90281-8.

[75] A. Guarnieri, G. Tolkmit, Millimeterwave Spectrum and Centrifugal Distortion Analysis of Fluoroacetonitrile in the Ground State, Zeitschrift Naturforschung Teil A 39 (1984) 853–857. doi:10.1515/zna-1984-0905.

[76] K. Tanaka, T. Okabayashi, T. Tanaka, Microwave spectroscopy of fcccn in the ground and excited vibrational states, Journal of Molecular Spectroscopy 132 (1988) 467–476. doi:https://doi.org/10.1016/0022-2852(88)90340-2.

[77] R. J. Saykally, P. G. Szanto, T. G. Anderson, R. C. Woods, The microwave spectrum of hydrogen isocyanide., The Astrophysical Journal letter 204 (1976) L143–L145. doi:10.1086/182074.

[78] H. Jones, V. Typke, Analysis of centrifugal distortion effects in the rotational spectrum of formyl fluoride, Zeitschrift für Naturforschung A 36 (1981) 1057–1061. doi:doi:10.1515/zna-1981-1006.

[79] J. Carpenter, The microwave spectrum and structure of carbonyl fluoride, Journal of Molecular Spectroscopy 50 (1974) 182–201. doi:https://doi.org/10.1016/0022-2852(74)90226-4.

Pure Rotational Spectroscopy Of The CH_2CN Radical Extended To The Sub-Millimeter Wave Spectral Region

OLIVIA CHITARRA[1], OLIVIER PIRALI[1], JEAN-THIBAUT SPANIOL[1], THOMAS HEARNE[1], JEAN-CHRISTOPHE LOISON[2], JOHN F. STANTON[3], AND MARIE-ALINE MARTIN-DRUMEL[1]

[1] *Université Paris-Saclay, CNRS, Institut des Sciences Moléculaires d'Orsay, 91405 Orsay, France*
[2] *Université Bordeaux, CNRS, Institut des Sciences Moléculaires, 33400 Talence, France*
[3] *Quantum Theory Project, Department of Chemistry, University of Florida, Gainesville, Florida 32611, USA*

Contact corresponding author(s): olivia.chitarra@universite-paris-saclay.fr
marie-aline.martin@universite-paris-saclay.fr

Supporting Information For Publication

LIST OF FIGURES

LIST OF TABLES

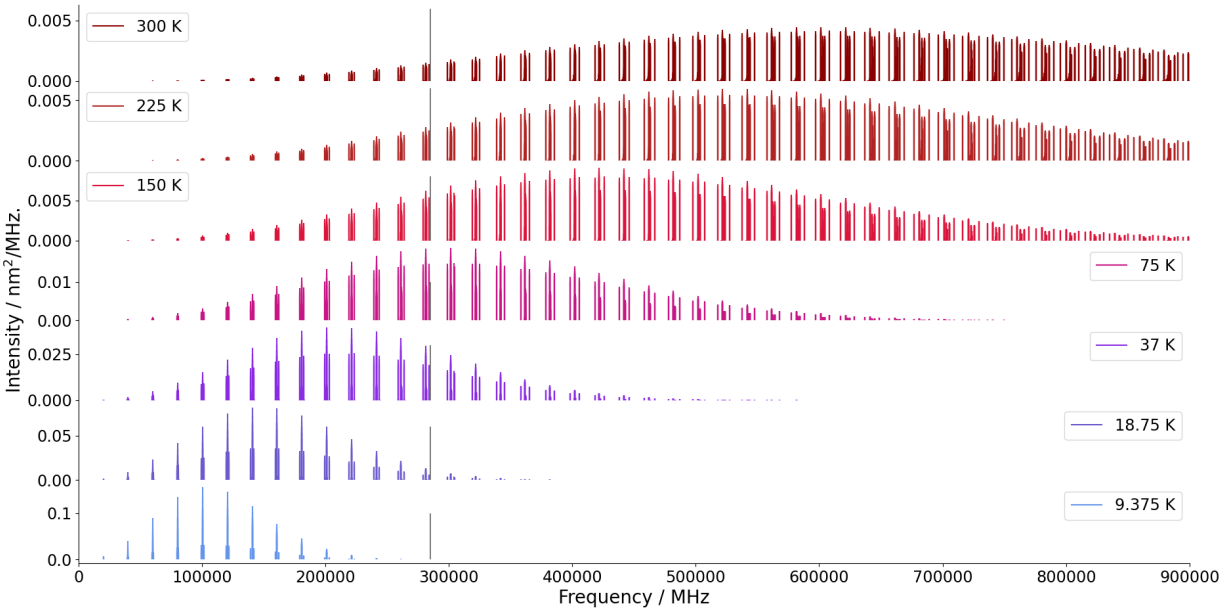

Fig. S1. Predictions of the rotational spectrum of the CH_2CN radical at different temperatures ranging from 10 K (lowest panel, in light blue) to 300 K (uppermost panel, in red) using the final set of rotational parameters. Note that the vertical grey line corresponds to the highest frequencies recorded by Ref. [2]. The list of partition functions used are provided in [4].

Table S1. Spectroscopic parameters (in MHz, unless otherwise noted) of CH_2CN in the Watson *A*-reduction determined in the literature [1] and from this work (Refit and Final). Numbers in parentheses are one standard deviation in units of the least significant figure.

Parameters [a]		Ref. [1]	Calc.	Refit	Final
Rotational parameters					
A		284981 [b]	285022	284981[b]	284975.1 (39)
B		10246.7658 (99)	10248	10246.69610 (56)	10246.7578 (18)
C		9876.0299 (73)	9877	9876.09860 (56)	9876.0372 (18)
Rotational centrifugal distortion constants					
Δ_N	$\times10^3$	4.063 (70)	3.87	4.02560 (90)	4.04678 (35)
Δ_{NK}	$\times10^3$	416.26 (85)	428	416.145 (97)	415.195 (56)
Δ_K		23.536 [c]	20.7	20.7	20.7[d]
δ_N	$\times10^3$	0.1611 [b]	0.140	0.1647 (13)	0.16405 (16)
δ_K		0.263 [b]	0.233	0.233	0.26200 (86)
Φ_N	$\times10^9$		−0.291	−0.291	−1.24 (12)
Φ_{NK}	$\times10^6$		4.76	4.76	0.827 (38)
Φ_{KN}	$\times10^3$	−0.719 [b]	−1.05	−0.7019 (77)	−0.8433 (46)
Φ_K	$\times10^3$	−2.4 [b]	5.86	5.86	5.86
ϕ_N	$\times10^9$		0.08	0.08	
ϕ_{NK}	$\times10^6$		2.44	2.44	
ϕ_K	$\times10^3$	−2.4 [b]	1.37	1.37	
L_{NK}	$\times10^6$	0.115 [b]			0.0170 (18)
L_{KKN}	$\times10^6$	−8.93 [b]		−8.80 (16)	−0.74 (13)
P_{KKNN}	$\times10^9$				0.833 (21)
P_{KKKN}	$\times10^6$				−0.1262 (11)
Electron spin-rotation and higher order terms					
ε_{aa}		−661.537 (20)	-697	−661.5481 (82)	−661.5287 (84)
ε_{bb}		−24.1205 (42)	-23.7	−24.1171 (47)	−24.1118 (46)
ε_{cc}		−2.035 (22)	1.43	−2.0401 (47)	−2.0384 (46)
$\Delta_S(K)$		0.14[b]		0.14[b]	0.0993(14)
$\Delta_S(KN)$		0.0105[b]		0.0105[b]	
isotropic and anisotropic hyperfine interaction constants					
a_F(N)		9.4866 (37)	7.19	9.4897 (17)	9.4905 (17)
T_{aa}(N)		−15.6386 (73)	-14.8	−15.6449 (32)	−15.6451 (32)
T_{bb}(N)		−12.4519 (96)	-13.5	−12.4731 (42)	−12.4734 (42)
χ_{aa}(N)		−4.1950 (89)	-4.26	−4.1953 (40)	−4.1959 (40)
χ_{bb}(N)		1.833 (13)	1.89	1.8171 (60)	1.8167 (60)
C_{aa}(N)		0.0273 (70)	-0.0275	-0.0275	-0.0275
C_{bb}(N)	$\times10^3$	2.9 (23)	-0.0021	-0.0021	-0.0021
C_{cc}(N)	$\times10^3$		-0.0023	-0.0023	-0.0023
a_F(H)[f]		−59.630 (33)	-56.9	−59.639 (13)	−59.644 (13)
T_{aa}(H)[f]		−15.9006 (68)	-17.1	−15.8966 (28)	−15.8965 (28)
T_{bb}(H)[f]		14.6 (67)	16.0	16.0	16.0
T_{bc}(H)[d]		1.15	1.15	1.15[d]	
Relevant fit parameters					
n[g]		545(206)		545(206)	545(207)+5260(801)
$N''_{\max}, K''_{a\max}$[h]		13,6		13,6	42,8
rms				0.03	0.15
σ[i]				1.77	1.20

[a] Parameters with no numerical values have not been used in the fit (i.e., fixed to 0) [b] Fixed at the value determined by Ref. [2]. [c] fixed at the value determined by Ref. [3] [d] Fixed at the calculated value. [e] Fixed at the value determined by Ref. [1]. [f] $X(\mathrm{H}) = X(\mathrm{H1}) = X(\mathrm{H2})$ for a given parameter X . [g] Number of fitted transitions (recorded frequencies). In the present fit, the number of newly measured lines and lines from the literature [1, 2] are reported, respectively. [h] unitless [i] Weighted standard deviation, unitless

REFERENCES

1. H. Ozeki, T. Hirao, S. Saito, and S. Yamamoto. Laboratory microwave spectroscopy of the cyanomethyl radical, CH_2CN. *The Astrophysical Journal*, **617**(1), 680–684 (2004). doi:10.1086/425229.
2. S. Saito and S. Yamamoto. The microwave spectrum of the cyanomethyl radical $CH_2CN(^2B_1)$. *The Journal of Chemical Physics*, **107**(6), 1732–1739 (1997). doi:10.1063/1.475154.
3. J. Johns, J. Stone, and G. Winnewisser. The ground state of ketene. *Journal of Molecular Spectroscopy*, **42**(3), 523–535 (1972). doi:10.1016/0022-2852(72)90227-5.
4. C. P. Endres, S. Schlemmer, P. Schilke, J. Stutzki, and H. S. Müller. The cologne database for molecular spectroscopy, cdms, in the virtual atomic and molecular data centre, vamdc. *Journal of Molecular Spectroscopy*, **327**, 95–104 (2016). New Visions of Spectroscopic Databases, Volume II. URL: https://www.sciencedirect.com/science/article/pii/S0022285216300340, doi:https://doi.org/10.1016/j.jms.2016.03.005.